



**HAL**  
open science

## Theoretical insights into multibandgap hybrid perovskites for photovoltaic applications

Jacky Even, Daniel Saponi, Laurent Pedesseau, Alain Rolland, Mikael Kepenekian, Roberto Robles, Shijian Wang, Yong Huang, Alexandre Beck, Olivier Durand, et al.

### ► To cite this version:

Jacky Even, Daniel Saponi, Laurent Pedesseau, Alain Rolland, Mikael Kepenekian, et al.. Theoretical insights into multibandgap hybrid perovskites for photovoltaic applications. Proceedings of SPIE, the International Society for Optical Engineering, 2015, Carbon Nanotubes, Graphene, and Emerging 2D Materials for Electronic and Photonic Devices VIII, 9552, pp.95520Z. <10.1117/12.2191953>. <hal-01417661>

**HAL Id: hal-01417661**

**<https://univ-rennes.hal.science/hal-01417661v1>**

Submitted on 15 Dec 2016

**HAL** is a multi-disciplinary open access archive for the deposit and dissemination of scientific research documents, whether they are published or not. The documents may come from teaching and research institutions in France or abroad, or from public or private research centers.

L'archive ouverte pluridisciplinaire **HAL**, est destinée au dépôt et à la diffusion de documents scientifiques de niveau recherche, publiés ou non, émanant des établissements d'enseignement et de recherche français ou étrangers, des laboratoires publics ou privés.



HAL Authorization

## Theoretical insights into multibandgap hybrid perovskites for photovoltaic applications

Jacky Even<sup>\*a</sup>, Daniel Saporì<sup>a</sup>, Laurent Pedesseau<sup>a</sup>, Alain Rolland<sup>a</sup>, Mikael Kepenekian<sup>b</sup>, Roberto Robles<sup>c</sup>, Shijian Wang<sup>a</sup>, Yong Huang<sup>a</sup>, Alexandre Beck<sup>a</sup>, Olivier Durand<sup>a</sup>, C. Katan<sup>b</sup>

<sup>a</sup>Université Européenne de Bretagne, INSA, FOTON UMR 6082, 35708 Rennes, France; <sup>b</sup>Institut des Sciences Chimiques de Rennes, UMR 6226, CNRS – Université de Rennes 1, France; <sup>c</sup>ICN2 - Institut Catala de Nanociencia i Nanotecnologia, Campus UAB, 08193 Bellaterra (Barcelona), Spain

### ABSTRACT

This paper reviews some of the recent theoretical investigations on the Rashba Dresselhaus spin effects and dielectric properties of  $\text{CH}_3\text{NH}_3\text{PbI}_3$  hybrid perovskites and  $\text{CsPbI}_3$  all-inorganic perovskites using Density functional theory. The spin vectors rotate in the non-centrosymmetric  $P4mm$  tetragonal phase, respectively clockwise and counterclockwise, in a manner that is characteristic of a pure Rashba effect. The high frequency dielectric constants  $\epsilon_\infty$  of  $\text{MAPbI}_3$  and  $\text{CsPbI}_3$  are similar as anticipated, since large differences are only expected at very low frequency where additional contributions from molecular reorientations show off for the hybrid compounds. A first simulation of a perovskite on silicon tandem cell, including a tunnel junction, is also investigated. Effect of halogen substitution (I/Br) is inspected, revealing limitations for short-circuit current and open-circuit voltage electrical characteristics.

**Keywords:** hybrid perovskite, solar cell, rashba, tandem, silicon, dielectric

### 1. INTRODUCTION

A scientific breakthrough for solar cells was achieved in the last three years using 3D Hybrid Organic Perovskites (HOP) with the chemical formulae  $\text{MAMX}_3$ , where MA is an organic cation  $\text{CH}_3\text{NH}_3^+$ , X is a halogen atom (X=I, Br, Cl) and M a metal atom (M=Pb, Sn). The efficiency of hybrid perovskites solar cells rose rapidly from 3.8% in 2009 with DSSC-like technologies to about 10% in 2012 using new concepts. These record values steeply increased to about 15% in 2013 thanks to new deposition techniques. At the end of 2014, optimized conversion efficiency amounts to 19.3% and then 20% in the last (2014) NREL efficiency chart. Over 21% efficiency was announced for a perovskite on silicon tandem cell at the HOPV Roma conference in May 2015. Clearly, understanding physical properties of operational HOPs and the design of novel devices with improved performances will greatly benefit from theoretical work. Prior to 2013, most theoretical studies either focused on layered HOP, purely inorganic 3D perovskites, and 3D HOP, but, in the latter case, missing inherent physical properties such as effect of spin-orbit coupling. In 2013, a few theoretical papers have appeared on 3D HOP in relation with the breakthrough in the field of photovoltaics, followed by a large number of papers in 2014. Significant progress has been made toward a better understanding of the unusual physical properties of this new class of semiconductors. This paper reviews some of the recent theoretical investigations using the SIESTA Density functional theory code that may contribute to gain better physical understanding of HOP materials, especially focusing on  $\text{MAPbX}_3$  compounds. Besides, a primary study of a perovskite on silicon tandem cell, including a tunnel junction, is presented, based on the SILVACO code dedicated to optoelectronic device simulation.

### 2. ELECTRONIC PROPERTIES AND RASHBA DRESSELHAUS SPIN INTERACTION

A giant spin-orbit coupling (SOC) operates on the conduction band (CB) of lead-based HOPs, leading to SOC splittings consistent with metal atomic energy level tables and to a spin-orbit split-off state at the bottom of the CB (figure 1). The optical transitions are related to a direct electronic band gap located at the R point of the Brillouin zone (BZ) of the reference high temperature  $Pm\bar{3}m$  centrosymmetric cubic phase. Besides SOC, time reversal symmetry (T-symmetry) is also important for spin effects, whether or not combined with inversion symmetry close to high symmetry points. For conjugated spinor states, T-symmetry yields the general conditions:  $E_n\uparrow(\mathbf{k})=E_n\downarrow(-\mathbf{k})$  and  $E_n\downarrow(\mathbf{k})=E_n\uparrow(-\mathbf{k})$ . Inversion

\*jacky.even@insa-rennes.fr

symmetry yields additional conditions:  $E_{n\uparrow}(k)=E_{n\uparrow}(-k)$  and  $E_{n\downarrow}(k)=E_{n\downarrow}(-k)$ . Combining both symmetries leads to a double spin degeneracy,  $E_{n\uparrow}(k)=E_{n\downarrow}(k)$ , across all the dispersion diagram within the BZ of the Pm-3m crystal structure. However, the room (high)-temperature crystal structure of 3D lead-based hybrid perovskites remains under debate. Recent single crystal X-ray diffraction experiments, performed on MAPbI<sub>3</sub> close to room temperature, support a non-centrosymmetric tetragonal space group (P4mm), which might lead at low temperature to another non-centrosymmetric I4cm tetragonal phase. A first effect of the Pm-3m to P4mm space group change is the folding of the CB and valence band (VB) states from the R-point to the A point (figure 1). Besides electronic band folding effect, the most important transformation of the diagram is due to atomic displacements. Lattice tetragonal strain leads to an increase of the band gap and a partial splitting of the CB when the SOC is neglected.

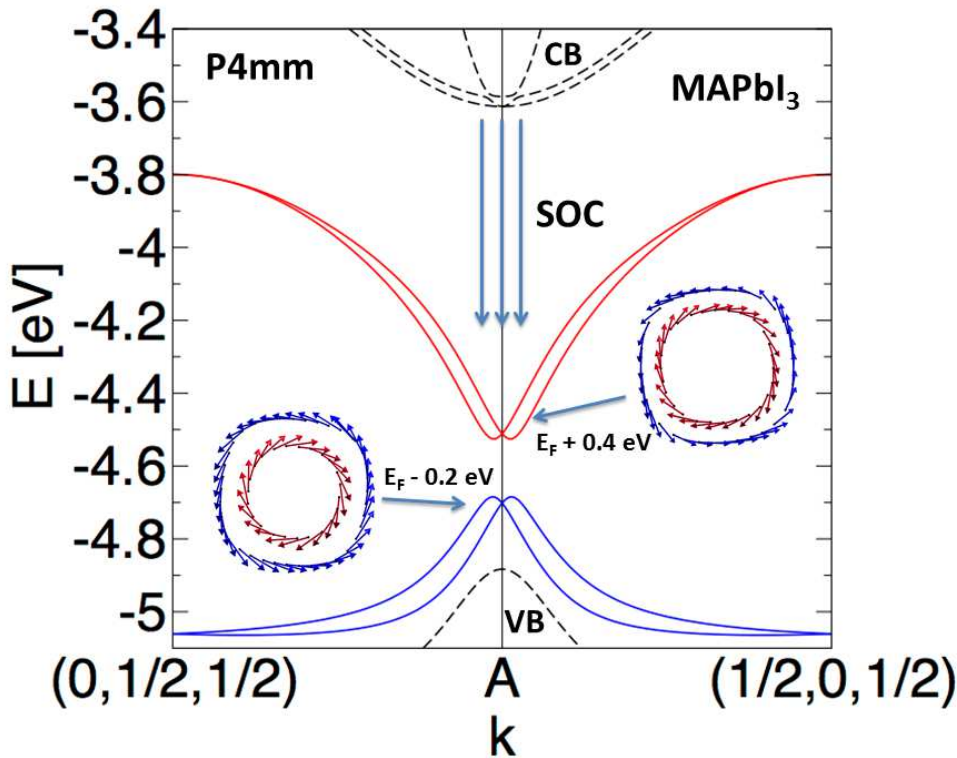


Figure 1. Electronic band structure of MAPbI<sub>3</sub> in the P4mm crystal phase with (straight lines) and without (dotted lines) the spin-orbit coupling (SOC) interaction. The downward shift of the CB is indicated by three arrows. The spin vectors rotate, in the CB and the VB, respectively clockwise and counterclockwise on the inner and outer circles, in the typical manner of pure Rashba effect (DFT computation with the GGA functional and the SIESTA code).

When inversion symmetry is lost in the P4mm phase, the spin degeneracy condition  $E_{n\uparrow}(k)=E_{n\downarrow}(k)$  is lost as well for a general wave vector, except for special high symmetry points like the A-point (figure 1). In 3D HOPs, it has been shown that even a small P4mm and I4cm symmetry breaking can lead to a strong spinor splitting, since the SOC effect is giant, as compared to conventional semiconductors. Such a k-dependent band splitting, also designated under Rashba/Dresselhaus, Dresselhaus, and Rashba effect, was confirmed by many theoretical groups, but still deserves experimental evidence in HOP. Indeed, the electronic band diagram of the P4mm phase of CH<sub>3</sub>NH<sub>3</sub>PbI<sub>3</sub> close to the critical point A of the BZ exhibits a splitting of the spinor bands. This effect is larger in the tetragonal I4cm phase. A linear mixed Rashba-Dresselhaus effect close to a degenerate high symmetry point can be studied by considering the spin-dependent Hamiltonian:

$$\hat{H}_{RD} = \lambda_R(k_x \hat{\sigma}_y - k_y \hat{\sigma}_x) + \lambda_D(k_x \hat{\sigma}_y + k_y \hat{\sigma}_x)$$

where  $\lambda_R$  and  $\lambda_D$  are constants related to the magnitudes of the Rashba and Dresselhaus terms, respectively. For the Amm2 space group, both terms coexist, but  $\lambda_D$  vanishes by symmetry for the P4mm case. Thus, the wavefunctions eigenvectors can be computed for the P4mm bands close to the A-point as:

$$\Psi_{R\pm} = \frac{e^{ik_t \cdot r}}{2\pi\hbar\sqrt{2}} \begin{vmatrix} 1 \\ \mp ie^{i\theta} \end{vmatrix}$$

where  $k_t$  and  $\theta$  are the wavevector and wavevector orientation angle, in the ( $k_x, k_y$ ) plane. A classical representation of the the splitted spin states is afforded by the expectations  $\langle \sigma \rangle$  vectors of the  $\sigma = (\sigma_x, \sigma_y, \sigma_z)$  vector of Pauli spin matrices for the two eigenvectors. Each  $\langle \sigma \rangle$  spin vector is represented by a small arrow at a point defined by the corresponding eigen-energy and  $\theta$ . Such a computation was performed for the CB and VB states of the P4mm phase of MAPbI<sub>3</sub> (figure 1). The spin vectors rotate respectively clockwise and counterclockwise on the inner and outer circles, in the typical manner of pure Rashba effect.

### 3. FIRST PRINCIPLES SIMULATION OF THE DIELECTRIC PROPERTIES

The dielectric constant is related to the response of the medium to local charges or external electric field, and thus plays an important role in the optoelectronic properties of hybrid perovskites. For MAPbI<sub>3</sub>, it has been shown experimentally that the high frequency dielectric constant  $\epsilon_\infty$  amounts to 6.5, and shows a smooth variation with temperature up to 20-30 in the medium frequency range (~90GHz). Comparison to purely inorganic 3D perovskites suggests that the difference between these two regimes stems from contributions related to polar optical phonons. Above the critical temperature  $T_c$ , the low frequency value (~1KHz) of  $\epsilon$  increases, and reaches about 60 at room temperature. We attributed this to the thermal activation of the collective tumblings of MA cations. Recently, giant dielectric constants have been reported in the low frequency regime: in the order 1000 in the dark and an additional factor of 1000 upon illumination under 1 sun. This effect has been attributed to very slowly moving photoinduced carriers assisted by molecular rotations.

Herein we apply a new DFT-based method, already tested for colloidal nanoplatelets of CdSe, to determine the high frequency dielectric constant  $\epsilon_\infty$  of MAPbI<sub>3</sub> and CsPbI<sub>3</sub>. The first step consists in the determination of the electronic density induced by an external electric field  $\mathbf{E}_{ext}$  applied to slabs in a direction ( $z$ ) perpendicular to the surface (figure 2). The induced polarization profile across the slab  $\mathbf{p}_{ind}(\mathbf{z})$  is thus computed from nanoscale average of the induced

charge density profile. Subsequently, the dielectric constant profiles are computed from:  $\epsilon(\mathbf{z}) = \frac{\epsilon_0 \mathbf{E}_{ext}}{\epsilon_0 \mathbf{E}_{ext} - \mathbf{p}_{ind}(\mathbf{z})}$  (figure 2).

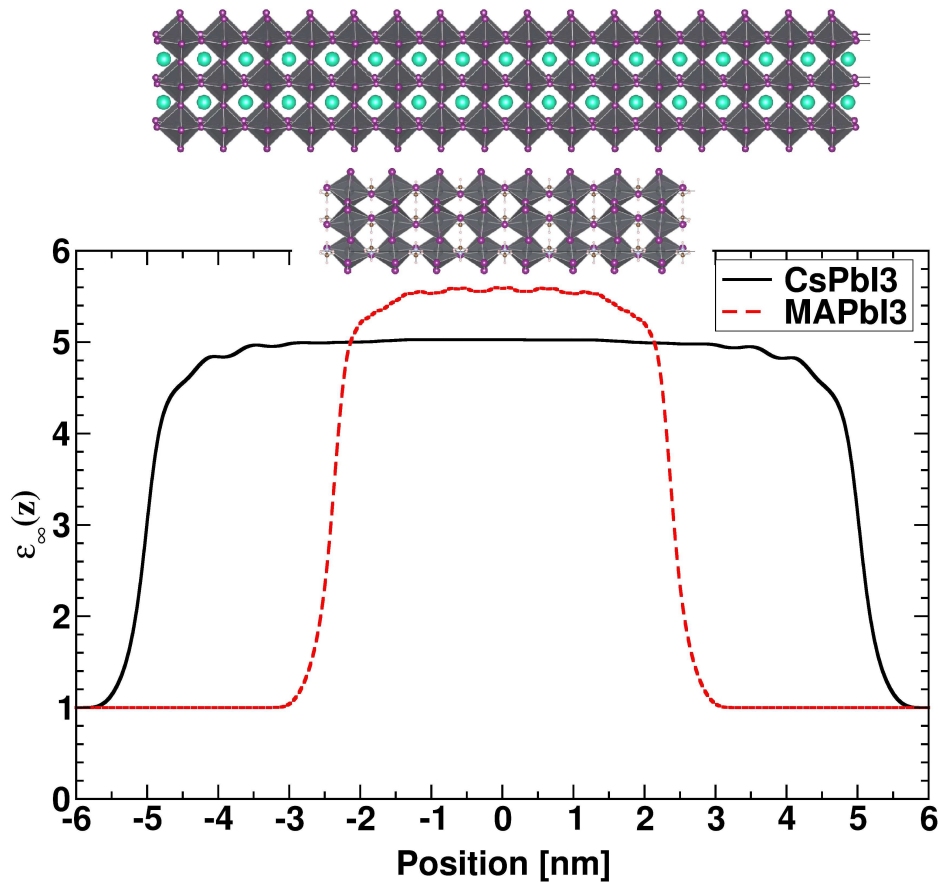


Figure 2. Nanoscale dielectric constant  $\epsilon_{\infty}(z)$  as a function of the position along the stacking axis ( $z$ ) for isolated slabs of MAPbI<sub>3</sub> (red dashed line) and CsPbI<sub>3</sub> (black straight line) in vacuum (DFT computation with the LDA functional and the SIESTA code).

$\epsilon_{\infty}$  amounts to 5.5 in the central part of the MAPbI<sub>3</sub> slab, in reasonable agreement with the experimental value (6.5) for the bulk compound at room temperature. The MAPbI<sub>3</sub> slab was built from the low-temperature orthorhombic Pnma phase, since the dynamical disorder of the MA cations in the Pm-3m phase prevents from using atomic positions for C, N, and H atoms in the DFT simulation without implicit bias. A small anisotropy of the dielectric constant in the Pnma phase is thus expected and might contribute to the difference between the theoretical and experimental estimates. The high frequency dielectric constant  $\epsilon_{\infty}$  for the CsPbI<sub>3</sub> compound is of the same order of magnitude (4.8). Indeed, it is related to a similar response of the electronic gas to the external field  $\mathbf{E}_{ext}$ . The two compounds should also exhibit similar values in the intermediate frequency range, where the ionic contribution yields an increase of the dielectric constant. However, at very low frequencies only the hybrid compound MAPbI<sub>3</sub> undergoes a further increase of the dielectric constant in relation with molecular dipoles reorientations.

#### 4. DRIFT-DIFFUSION MODELLING OF PEROVSKITE ON SILICON TANDEM SOLAR CELLS WITH TUNNEL JUNCTIONS

Single HOP cells have been used to demonstrate over 20% solar to electricity conversion efficiency. One attractive solution to further enhance these performances is to stack multiple solar cell junctions, which combine absorbers with different electronic bandgaps to optimize solar light-harvesting. This concept has been recently tested in a tandem configuration, using either CIGS or silicon as a small band-gap material and the MAPbI<sub>3</sub> HOP as a large band gap

material. In this paper, we present a numerical simulation of a two terminal perovskite-based tandem cell monolithically integrated on silicon (Si) and including a Si interband Tunnel Junction (TJ) to electrically interconnect the top and the bottom sub-cells (figure 3, left). The purpose of this preliminary study is to identify some key parameters of this architecture, as well as to explore the influence of HOP chemical engineering (figure 3, right).

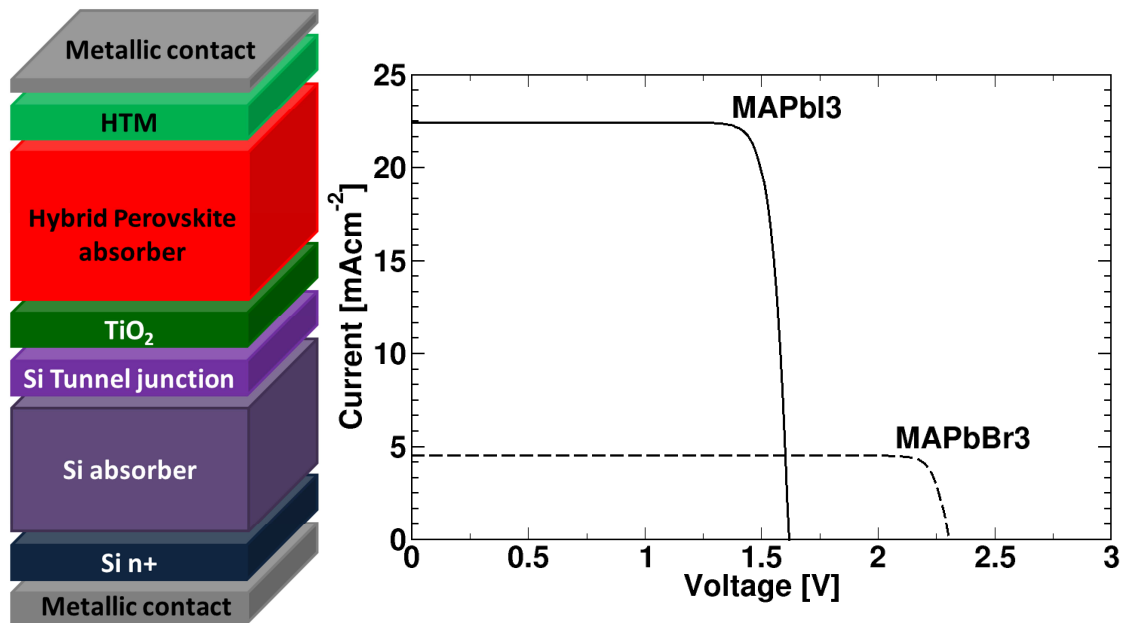


Figure 3. (left) structure of a perovskite tandem solar cell monolithically integrated on n-doped silicon substrate. (right) J-V characteristics of the tandem cell including either the iodine MAPbI<sub>3</sub> (straight line) or the bromide MAPbBr<sub>3</sub> (dashed line) hybrid perovskite as an absorber.

Figure 3 shows the device structure of the perovskite tandem solar cell monolithically integrated on a n-type silicon substrate. The structure consists in a 850 nm thick Hole Transport Material layer (HTM), a perovskite methyl ammonium MAPbX<sub>3</sub> lead tri-iodide (X=I) or tri-bromide (X=Br) absorbing layer, a 300 nm thick TiO<sub>2</sub> electron transport layer, a 2x20 nm thick Si(n<sup>+</sup>)/Si(p<sup>+</sup>) tunnel junction, a 280 μm thick n-type Si substrate and a 100 nm thick heavily n-doped Si layer for the backside contact. The doping level for the silicon tunnel junction has been set to 10<sup>20</sup> cm<sup>-3</sup>. This doping level ensures a nice electrical serial connection between the top perovskite cell and the bottom Si cell. The classical tunnel junction model implemented in the Silvaco Atlas device simulator was used. An identical single Si cell exhibits an efficiency of 15% under AM1.5 illumination, with a short-circuit current density J<sub>SC</sub> = 49.0 mAcm<sup>-2</sup> and an open-circuit voltage V<sub>OC</sub> = 0.50 V. For the HOP materials, n-type and p-type carrier mobilities were set to 2 cm<sup>2</sup>V<sup>-1</sup>s<sup>-1</sup> in agreement with previous perovskite solar cell modeling. The single MAPbI<sub>3</sub> (MAPbBr<sub>3</sub>) cell efficiency amounts to 13% (6%) under AM1.5 illumination, with a short-circuit current density J<sub>SC</sub> = 22.0 mAcm<sup>-2</sup> (6.0 mAcm<sup>-2</sup>) and an open-circuit voltage V<sub>OC</sub> = 0.85 V (1.7V). By comparing the short-circuit current densities of single Si and perovskite cells, we can already conclude that the perovskite cell limits the current especially in the case of MAPbBr<sub>3</sub> HOP material. The tandem cell short circuit current limitation is expected to be compensated by an enhancement of the V<sub>oc</sub> for the whole structure. Figure 3 (right) shows that for the MAPbI<sub>3</sub> based tandem cell, the short circuit current is indeed limited by the perovskite part of the structure, however a large V<sub>oc</sub> (1.6V) is obtained. The tandem cell efficiency is thus increased to a value of 17%, larger than the values of 13% (MAPbI<sub>3</sub>) and 15% (Si) for each single cell. On the other hand, the drastic reduction of the short-circuit current in the MAPbBr<sub>3</sub> based tandem cell (figure 3, right) with respect to a single Si solar cell, is not fully compensated by the very large value of V<sub>oc</sub>. The tandem cell efficiency in this configuration is indeed equal to 11%, and thus does not exhibit any improvement by comparison to a single Si solar cell.

## 5. CONCLUSION

This review shows that density functional theory (DFT) and empirical drift-diffusion models are useful tools for studying the optoelectronic properties of HOP compounds. The giant Rashba spin splitting is predicted for the MAPbI<sub>3</sub> in the tetragonal phase from DFT simulation in good agreement with symmetry-based model Hamiltonian. High-frequency dielectric constant profiles are determined for perovskite slabs, using DFT computation. Nanoscale averaging is performed in order to achieve a comparison with experimental values for bulk dielectric constants. A first device simulation of HOP on silicon tandem solar cell is described. This study gives some indications about the key parameters that may lead to an optimization of tandem cell performances, including the chemical engineering afforded by the HOP compounds.

## REFERENCES

- [1] Mitzi, D. B., Wang, S., Field, C. A., Chess, C. A. and Guloy, A. M., "Conducting Layered Organic-inorganic Halides Containing <110>-Oriented Perovskite Sheets," *Science*, 267, 1473-1476 (1995).
- [2] Kagan, C. R., Mitzi, D. B. and Dimitrakopoulos, C. D., "Organic-inorganic hybrid materials as semiconducting channels in thin-film field-effect transistors," *Science*, 286, 945-947 (1999).
- [3] Kojima, A., Teshima, K., Shirai, Y. and Miyasaka, T., "Organometal Halide Perovskites as Visible-Light Sensitizers for Photovoltaic Cells," *J. Am. Chem. Soc.* 131 (17), 6050-6051 (2009).
- [4] Im, J. H., Lee, C. R., Lee, J. W., Park, S. W. and Park, N. G., "6.5% Efficient Perovskite Quantum-Dot-Sensitized Solar Cell," *Nanoscale*, 3(10), 4088-4093 (2011).
- [5] Park, N. G., "Organometal perovskite light absorbers toward a 20% efficiency low-cost solid-state mesoscopic solar cell," *J. Phys Chem. Lett.* 4, 2423-2429 (2013).
- [6] Snaith, H. J., "Perovskites: The emergence of a new era for low-cost, high-efficiency solar cells," *J. Phys Chem. Lett.* 4, 3623-3630 (2013).
- [7] Kim, H. S., Lee, C. R., Im, J. H., Lee, K. B., Moehl, T., Marchioro, A., Moon, S. J., Humphry-Baker, R., Yum, J. H., Moser, J. E., Grätzel, M. and Park, N-G., "Lead Iodide Perovskite Sensitized All-Solid-State Submicron Thin Film Mesoscopic Solar Cell with Efficiency Exceeding 9%," *Sci. Rep.* 2, 591-591-7 (2012).
- [8] Lee, M. M., Teuscher, J., Miyasaka, T., Murakami, T. N. and Snaith, H. J., "Efficient Hybrid Solar Cells Based on Meso-Superstructured Organometal Halide Perovskites," *Science* 338, 643-647 (2012).
- [9] Burschka, J., Pellet, N., Moon, S. J., Humphry-Baker, R., Gao, P., Nazeeruddin, M.K. and Grätzel, M., "Sequential deposition as a route to high-performance perovskite-sensitized solar cells," *Nature* 499, 316-319 (2013).
- [10] Liu, M., Johnston, M. B. and Snaith, H. J., "Efficient planar heterojunction perovskite solar cells by vapour deposition," *Nature* 501, 395-398 (2013).
- [11] Xing, G., Mathews, N., Sun, S., Lim, S. S., Lam, Y. M., Grätzel, M., Mhaisalkar, S. and Sum, T. C., "Long-range balanced electron- and hole-transport lengths in organic-inorganic CH<sub>3</sub>NH<sub>3</sub>PbI<sub>3</sub>," *Science* 342, 344-347 (2013).
- [12] Stranks, S. D., Eperon, G. E., Grancini, G., Menelaou, C., Alcocer, M. J. P., Leijtens, T., Herz, L. M., Petrozza, A. and Snaith, H. J., "Electron-hole diffusion lengths exceeding 1 micrometer in an organometal trihalide perovskite absorber," *Science* 342, 341-344 (2013).
- [13] Even, J., Pedesseau, L., Dupertuis, M.-A., Jancu, J.-M. and Katan, C., "Electronic model for self-assembled hybrid organic/perovskite semiconductors: Reverse band edge electronic states ordering and spin-orbit coupling," *Phys. Rev. B.* 86, 205301-1-205301-4 (2012).
- [14] Mosconi, E., Amat, A., Nazeeruddin, Md. K., Grätzel, M. and De Angelis, F., "First-principles modeling of mixed halide organometal perovskites for photovoltaic applications," *J. Phys. Chem. C* 117, 13902-13913 (2013).
- [15] Even, J., Pedesseau, L., Jancu, J.-M. and Katan, C., "Importance of spin-orbit coupling in hybrid organic/inorganic perovskites for photovoltaic applications," *J. Phys. Chem. Lett.* 4, 2999-3005 (2013).
- [16] Brivio, F., Walker, A. B., Walsh, A., "Structural and electronic properties of hybrid perovskites for high-efficiency thin-film photovoltaics from first-principles," *Appl. Phys. Lett.* Mat. 1, 042111-1-042111-5 (2013).
- [17] Giorgi, V., Fujisawa, J.-I., Segawa, H., Yamashita, K., "Small photocarrier effective masses featuring ambipolar transport in methylammonium lead iodide perovskite: A density functional analysis," *J. Phys. Chem. Lett.* 4, 4213-4216 (2013).
- [18] Yin, W.-J., Shi, T., and Yan, Y., "Unusual defect physics in CH<sub>3</sub>NH<sub>3</sub>PbI<sub>3</sub> perovskite solar cell absorber," *Appl. Phys. Lett.* 104, 063903-1-063903-4 (2014).

- [19] Even, J., Pedesseau, L., Jancu, J.-M. and Katan, C., "Importance of spin-orbit coupling in hybrid organic/inorganic perovskites for photovoltaic applications," *J. Phys. Chem. Lett.* 4, 2999-3005 (2013).
- [20] Pedesseau, L., Jancu, J.-M., Rolland, A., Deleporte, E., Katan, C., and Even, J., "Electronic properties of 2D and 3D hybrid organic/inorganic perovskites for optoelectronic and photovoltaic applications," *Opt. Quant. Electron.* 46, 1225-1232 (2014).
- [21] Even, J., Pedesseau, L. and Katan, C., "Analysis of multivalley and multibandgap absorption and enhancement of free carriers related to exciton screening in hybrid perovskites," *J. Phys. Chem. C* 118, 11566-11572 (2014).
- [22] Even, J., Pedesseau, L. and Katan, C., "Understanding quantum confinement of charge carriers in layered 2D hybrid perovskites," *ChemPhysChem*. 15, 3733-3741 (2014).
- [23] Katan, C., Pedesseau, L., Kepenekian, M., Rolland, A. and Even, J., "Interplay of spin-orbit coupling and lattice distortion in metal substituted 3D tri-chloride hybrid perovskites," *J. Mater. Chem. A* 3, 9232-9240 (2015).
- [24] Even, J., Pedesseau, L., Katan, C., Kepenekian, M., Lauret, J.-S., Saponi, D., and Deleporte, E., "Solid-State Physics Perspective on Hybrid Perovskite Semiconductors," *J. Phys. Chem. C* 119, 10161-10177 (2015).
- [25] Even, J., "Pedestrian Guide to Symmetry Properties of the Reference Cubic Structure of 3D All-inorganic and Hybrid Perovskites," *J. Phys. Chem. Lett.* (2015).
- [26] Soler, J. M., Artacho, E., Gale, J. D., Garcia, A., Junquera, J., Ordejon P. and Sanchez-Portal, D., "The SIESTA method for ab initio order-N materials simulation." *J. Phys.: Condens. Matter*, 14, 2745 (2002).
- [27] Silvaco Inc., ATLAS user's manual, Sunnyvale, CA, <http://silvaco.com> 2012.
- [28] Winkler, R.; [Spin-orbit Coupling Effects in Two-Dimensional Electron and Hole Systems]. *New-York: Springer Tracts in Modern Physics*, Springer-Verlag.(2004)
- [29] Even, J., Pedesseau, L., Jancu, J.-M. and Katan, C., "DFT and  $k \cdot p$  modelling of the phase transitions of lead and tin halide perovskites for photovoltaic cells," *Phys. Status Solidi RRL* 8, 31-35 (2014).
- [30] Amat, A., Mosconi, E., Ronca, E., Quarti, C., Umari, P., Nazeeruddin, M. K., Grätzel, M., De Angelis, F., "Cation-Induced Band-Gap Tuning in Organohalide Perovskites: Interplay of Spin-Orbit Coupling and Octahedra Tilting." *Nano Lett.* 14, 3608-3616 (2014).
- [31] Brivio, F., Butler, K. T., Walsh, A., van Schilfgaarde, M., "Relativistic quasiparticle self-consistent electronic structure of hybrid halide perovskite photovoltaic absorbers." *Phys. Rev. B*, 89, 155204 (2014).
- [32] Kim, M., Im, J., Freeman, A. J., Ihm, J., Jin, H., "Switchable  $S = 1/2$  and  $J = 1/2$  Rashba bands in ferroelectric halide perovskites." *PNAS*, 111, 6900-6904 (2014).
- [33] Stroppa, A., Di Sante, D., Barone, P., Bokdam, M., Kresse, G., Franchini, C., Whangbo, M.-H. and Picozzi, S., "Tunable ferroelectric polarization and its interplay with spin-orbit coupling in tin iodide perovskites," *Nature Commun.* 5, 5900 (2014).
- [34] Onoda-Yamamuro, N., Matsuo, T., Suga, H., "Dielectric study of  $\text{CH}_3\text{NH}_3\text{PbX}_3$  ( $X = \text{Cl, Br, I}$ )," *J. Phys. Chem. Solids* 53, 935-939 (1992).
- [35] Juarez-Perez, E. J., Sanchez, R. S., Badia, L. Garcia-Belmonte, G., Kang, Y. S., Mora-Sero, I., Bisquert, J., "Photoinduced Giant Dielectric Constant in Lead Halide Perovskite Solar Cells," *J. Phys. Chem. Lett.* 5, 2390-2394 (2014).
- [36] Fang, H.-H., Raissa, R., Abdu-Aguye, M., Adjokotse, S., Blake, G. R., Even, J. and Loi, M. A., "Photophysics of Organic-Inorganic Hybrid Lead Iodide Perovskite Single Crystals." *Adv. Func. Mater.* 25, 2378-2385 (2015).
- [37] Miyata, A., Mitioglu, A., Plochocka, P., Portugall, O., Tse-Wei Wang, J., Stranks, S.D., Snaith, H. J., Nicholas, R.J., "Direct Measurement of the Exciton Binding Energy and Effective Masses for Charge carriers in an Organic-Inorganic Tri-halide Perovskite," *Nature Phys.* 11, 582-587 (2015)
- [38] Even, J., Pedesseau, L., Kepenekian, M., "Electronic surface states and dielectric self-energy profiles in colloidal nanoscale platelets of  $\text{CdSe}$ ," *Phys. Chem. Chem. Phys.* 16, 25182-25190 (2014).
- [39] Benchamekh, R. N., Gippius, A., Even, J., Nestoklon, M. O., Jancu, J.-M., Ithurria, S., Dubertret, B., Efros, A. L., Voisin, P., "Tight-binding calculations of image-charge effects in colloidal nanoscale platelets of  $\text{CdSe}$ ," *Phys. Rev. B* 89, 035307 (2014).
- [40] Mailoa, J. P., Bailie, C. D., Johlin, E.C., Hoke, E.T., Akey, A.J., Nguyen, W. H., McGehee, M.D. and Buonassisi, T., "A 2-terminal perovskite/silicon multijunction solar cell enabled by a silicon tunnel junction," *Appl. Phys. Lett.* 106, 121105 (2015).
- [41] Minemoto, T., Murata, M., "Device modeling of perovskite solar cells based on structural similarity with thin film inorganic semiconductor solar cells," *J. Appl. Phys.* 116, 054505 (2014).
- [42] Rolland, A., Pedesseau, L., Even, J., Almosni, S., Robert, C., Cornet, C., Jancu, J.-M., Benhlal, J., Durand, O., Le Corre, A., Râle, P., Lombez, L., Guillemoles, J.-F., Tea, E. and Laribi, S., "Design of a lattice-matched III-V-N/Si

Proc. SPIE 9552, Carbon Nanotubes, 95520Z;  
doi:10.1117/12.2191953; <http://dx.doi.org/10.1117/12.2191953>

photovoltaic tandem cell monolithically integrated on silicon substrate," *Opt. Quant. Electron.* 46, 1397–1403 (2014).

[43] Minemoto, T., Murata, M., "Theoretical analysis on effect of band offsets in perovskite solar cells," *Solar Energy and Solar Cells.* 133, 8-14 (2015).